



## Determination of axial dispersion and overall mass transfer coefficients for Ni (II) adsorption on nanostructured $\gamma$ -alumina in a fixed bed column: experimental and modeling studies

Reyhane Saadi, Zahra Saadi, Reza Fazaeli\*

Faculty of Engineering, Department of Chemical Engineering, South Tehran Branch, Islamic Azad University, Tehran, Iran  
Tel. +982188303278; Fax: +9888830012; email: r\_fazaeli@azad.ac.ir

Received 19 June 2013; Accepted 26 October 2013

### ABSTRACT

In this study, nanostructured  $\gamma$ -alumina is used as an adsorbent for the removal of nickel from aqueous solutions using a fixed-bed column and batch experiments. Different parameters, including the initial nickel solution concentration, contact time, and pH were analyzed to determine their optimum values. The results showed that adsorption efficiency increased as contact time increased; optimum contact time was observed to be 150 min. The efficiency of removing metal ions from an aqueous solution increased as pH increased from 2.5 to 4.5, but decreased as pH rose higher, thus, optimum pH was determined to be 4.5. The Langmuir isotherm model showed better agreement with the experimental data than the Freundlich and Tempkin isotherm models. The maximum capacity of the adsorbent in the Langmuir equation was 78.74 mg/g. In the present study, adsorbent bed performance breakthrough curves for different adsorbent bed heights, influent flow rates, and concentrations were analyzed. The experimental data showed an increase in adsorption capacity at lower flow rates and higher influent concentrations and bed heights. To solve the bed equations, the lumped method was used to predict the breakthrough curve and model overall mass transfer coefficient ( $K_{\text{overall}}$ ) and axial dispersion coefficient ( $D_z$ ) parameters to compare with experimental results.

*Keywords:* Nickel; Nanostructured  $\gamma$ -alumina; Isotherm; Breakthrough curve; Dynamic modeling; Fixed-bed column

### 1. Introduction

Heavy metal ions dissolved in aqueous solutions are considered to be hazardous pollutants because of their toxicity, even at low concentrations [1]. These toxic metal ions commonly exist in process waste streams from mining operations, metal-plating

facilities, power generation facilities, electronic device manufacturing units, and tanneries [2–4].

Nickel is a heavy metal found in wastewater that may cause illnesses such as lung and bone cancer and result in extreme weakness, headache, dizziness, vomiting, chest pain, and shortness of breath [5]. According to the US Environmental Protection Agency, the maximum allowable concentration of nickel in drinking water is 0.1 mg/L [6]. Various methods exist for the removal of heavy metals, including ion exchange,

\*Corresponding author.

reverse osmosis, electrochemical operations, biological treatment, chemical precipitation, membrane filtration, oxidation, coagulation, and solvent extraction. These methods are often time-consuming, expensive, and inefficient.

Adsorption, however, has a simple design, is relatively inexpensive and has high removal efficiency, making it one of the most popular methods for the removal of heavy metals from aqueous solutions [7–13]. A number materials used to remove heavy metals from wastewater, such as activated carbon [14], natural and synthetic zeolite [15,16], alumina [17], chitosan [18], nanomaterials such as carbon nanotubes [19], nanometal-oxides [20] magnetic nanoparticles [21], lignite [22], biosorbents such as agricultural waste and biomass [23,24], have been investigated for the adsorption of heavy metals. Nanoalumina is a metallic oxide that is an important ceramic material.  $\gamma$ -alumina has more active sites on its surface than  $\alpha$ -alumina, and it has good mechanical strength, high thermal stability, and high surface area. Nanoalumina is widely used in chemical reactions as a catalyst, and in membrane processes and wastewater treatment [25–27].

Ghorai et al. [28] investigated the removal of fluoride ions using activated alumina in batch and continuous operations. A one-dimensional model for isothermal, axially dispersed fixed-bed adsorption was numerically solved and compared with their experimental results.

Adak et al. [29] investigated the removal of phenol from a water environment using surfactant-modified alumina. The adsorption capacity of an adsorbent was obtained at different bed heights, column diameters, constant concentration, and flow rates.

Hong et al. [30] studied the adsorption of Ni (II) on  $\gamma$ -type alumina using a differential bed reactor in aqueous solutions to determine its adsorption characteristics and overall adsorption rate.

Afkhami et al. [31] have studied the removal of metal cations Pb(II), Cd(II), Cr(III), Co(II), Ni(II), and Mn(II) from water samples using nanoalumina modified with 2,4-dinitrophenylhydrazine. Optimal experimental conditions for pH, adsorbent dosage, and contact time were established.

The present study evaluated the ability of nanostructured  $\gamma$ -alumina adsorbent to adsorb Ni(II) from aqueous solutions using the batch system and a fixed-bed column. The metal uptake and the effect of pH on the percentage of removal of metal ions were investigated. Langmuir, Freundlich and Tempkin isotherms were compared with the batch experimentation results. The effects of flow rate, initial concentration of nickel, and fixed-bed height on nickel adsorption were considered.

## 2. Materials and methods

### 2.1. Materials

Alumina nanoparticles with 99.9% purity were purchased from Nano-Pars Lima Co. All prepared materials had high purity, and deionized distilled water was used. Analytical grade Ni(NO<sub>3</sub>)<sub>2</sub> (Merck) was used without further purification. pH adjustments were performed using 0.1–1.0 mol/L HNO<sub>3</sub> and NaOH solutions. Heavy metal analysis was carried out using a PG 990 atomic absorption spectrophotometer. A digital pH meter (Sartorius PB-11) was used for pH measurement. Flow rates were regulated using a peristaltic pump (Etatron DS, Italy) capable of adjusting flow rates in the mL/min range.

### 2.2. Batch studies

Batch experiments were carried out in different sets using 20–110 mg/L nickel with an initial concentration of 160 mg/L in contact with 0.5 g of nanostructured  $\gamma$ -alumina at pH 4.5 for 150 min at room temperature. After 150 min of agitation to reach equilibrium conditions, the solid/liquid phases were separated by centrifuging at 10,000 rpm for 15 min. Nickel residual concentration in a transparent liquid was analyzed using an atomic absorption spectrophotometer. Batch equilibrium experiments determined an optimum pH values of 2.5–6.5 with an initial concentration of 20 mg/L in contact with 0.5 g of adsorbent. To evaluate the minimum time required to reach equilibrium, 25 min time intervals and an initial concentration of 20 mg/L was used. Concentration analysis was performed for up to 200 min.

The percentage of metal ion removed from aqueous solution by the adsorbent is expressed as Eq. (1):

$$R\% = \frac{C_0 - C_e}{C_0} \times 100 \quad (1)$$

$C_0$  is the initial concentration of the metal ions (mg/L), and  $C_e$  is the equilibrium concentration of metal ions (mg/L).

Regeneration studies were not done in the present research. The saturated adsorbent can be regenerated using chemical regeneration [32].

### 2.3. Column studies

A Pyrex column 30 cm in height and 1 cm in diameter was used for upward flow. The adsorption column was packed with spherical particles of

nanostructured  $\gamma$ -alumina between the two layers of glass wool. Fig. 1 shows a schematic of the experimental setup.

In order to investigate the effect of flow rate on the behavior of the adsorbent column, flow rates of 3, 6, and 9 mL/min at a constant concentration of 50 ppm, a constant bed height of 15 cm were used. Heights of 10, 15, and 20 cm (7.0585, 10.6028, and 14.1371 g) with a constant concentration 50 ppm and constant flow rate of 6 mL/min were used to investigate the effect of height on the behavior of the adsorbent column. To investigate the effect of initial concentration of the nickel ion on the behavior of the adsorbent column, concentrations of 30, 50, and 80 ppm at a constant bed height of 15 cm and constant flow rate of 6 mL/min were applied. For all experiments, sampling was done from the effluent solution at specified time intervals, and residual nickel concentration was measured by atomic absorption spectroscopy. All experiments were carried out at room temperature and pH 4.5.

The maximum adsorption capacity of the adsorbent in a fixed-bed column is calculated as Eqs. (2) and (3) [33]:

$$q_{\text{total}} = \frac{Q}{1,000} \int_0^{t_{\text{total}}} (C_0 - C_t) dt \quad (2)$$

$$q_{e, \text{max}} = \frac{q_{\text{total}}}{w} \quad (3)$$

where  $q_{e, \text{max}}$  is maximum adsorption capacity of the adsorbent (mg/g),  $Q$  is flow rate (mL/min),  $C_0$  is initial

concentration (mg/L),  $C_t$  is concentration in specified time (mg/L) and  $w$  is mass of the adsorbent (g).

### 3. Results and discussion

#### 3.1. Characterization of adsorbent

The spheres were made with is  $\gamma$ -alumina nanopowder with an average size of 20 nm. The resulting spheres are 2–3  $\mu\text{m}$  in diameter. The BET surface area is about 138  $\text{m}^2/\text{g}$  which exhibits good adsorption efficiency. The bulk density and porosity are 0.9  $\text{g}/\text{cm}^3$  and 0.5246, respectively. The chemical analysis of the adsorbent is presented in Table 1.

#### 3.2. Batch studies

##### 3.2.1. Effect of pH

The pH is important because it effects the removal of cations from the aqueous solution, since it determines the surface charge of the adsorbent and the degree of ionization of the adsorbate. To minimize the effect of nickel precipitation, the pH range was kept at 2.5–6.5. The effect of pH on adsorption efficiency is shown in Fig. 2. As seen, a pH of 4.5 provides maximum adsorption. Fig. 2 shows that the removal efficiency of Ni(II) increased as pH increased from 2.5 to 4.5 and decreased when the pH was greater than 4.5.

The adsorbent surface in contact with the aqueous solution from the formation of hydroxyl functional groups has a tendency to adsorb counter ions [34]. The extremely acidic environment and high concentration of protons at low pH creates

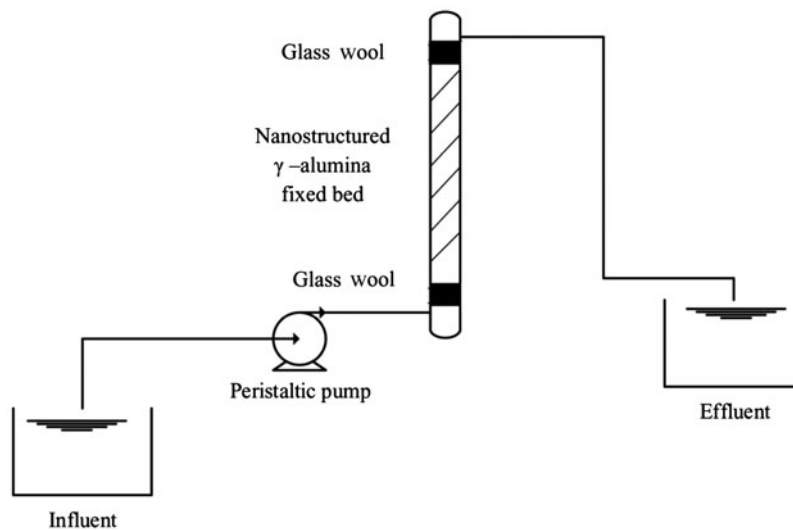


Fig. 1. Schematic diagram of the experimental column.

Table 1  
Chemical analysis of nanostructured  $\gamma$ -alumina

S. no	Chemical analysis	Value
1	Al <sub>2</sub> O <sub>3</sub> (minimum) %	99
2	Ca(maximum), ppm	25
3	V(maximum), ppm	7
4	CL(maximum), ppm	315
5	Na(maximum), ppm	70
6	Mn(maximum), ppm	3
7	Co(maximum), ppm	2

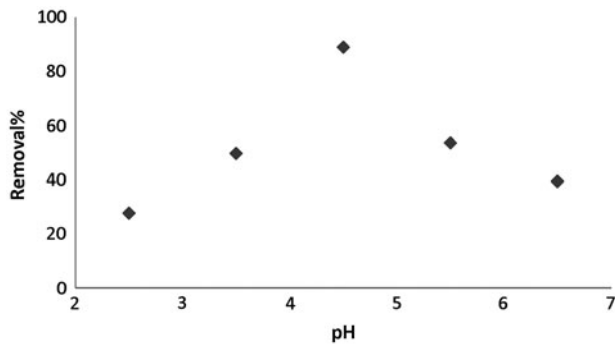


Fig. 2. Effect of pH on removal Ni (II) efficiency. Conditions: 0.5 g adsorbent, 100 mL of 20 mg/L of nickel.

competition between protons and metal ions for the occupation of active sites on the adsorbent and can decrease adsorption efficiency [35]. At a higher pH (4.5–6.5), the competition between active sites and hydroxide ions in interaction or reaction with nickel ions increased as hydroxide ion concentration increased. The formation of metal hydroxides and its precipitation leads to a decrease in adsorption efficiency. A higher pH of 6.5 caused by the formation of Ni (OH)<sub>2</sub> resulted in negligible adsorption of Ni<sup>2+</sup> species [36].

### 3.2.2. Effect of contact time

The time profile of Ni<sup>2+</sup> adsorption is plotted in Fig. 3. The removal efficiency of the metal ions reached maximum value after 150 min because of the vacant sites at the initial times, but adsorption then decreased as the number of active sites decreased, which finally led to a smooth curve.

### 3.2.3. Adsorption isotherms

Different isotherm equations have been developed to design and optimize the adsorption process and describe adsorbent behavior [37]. In this study,

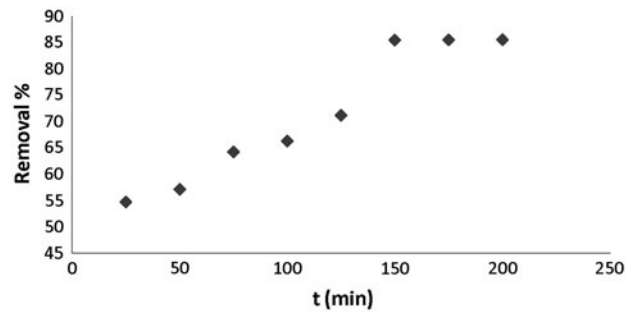


Fig. 3. Effect of contact time on removal Ni (II) efficiency. Conditions: 0.5 g adsorbent, 100 mL of 20 mg/L of nickel, pH 4.5.

experimental adsorption equilibrium data were evaluated using the Langmuir, Freundlich and Tempkin adsorption isotherm models. The equilibrium adsorption capacity of adsorbent was calculated as Eq. (4) [38]:

$$q_e = \frac{V(C_0 - C_e)}{W} \quad (4)$$

where  $q_e$  is the equilibrium adsorption capacity of adsorbent (mg/g),  $V$  is the volume of metal ions solution (L), and  $W$  is the weight of the adsorbent (g).

The Langmuir model assumes that the adsorbent surface is homogeneous, and adsorption energy is uniform for all sites and only a single layer of molecules on the adsorbent surface are absorbed [39]. The linear form of the Langmuir isotherm is expressed as Eq. (5) [39,40]:

$$\frac{1}{q_e} = \frac{1}{bq_m} \frac{1}{C_e} + \frac{1}{q_m} \quad (5)$$

where  $q_m$  is the maximum adsorption capacity (mg/g) of adsorbent.  $b$  is the equilibrium constant (L/mg) that is a criterion of the tendency of the metal to adsorb onto the active sites of the adsorbent surface. A larger  $b$  value represents higher adsorption energy. The  $q_m$  parameter was 78.74 mg/g, which shows the high adsorption capacity of the adsorbent. The dimensionless constant of the separation factor or equilibrium parameter to predict the adsorption efficiency and usability of the Langmuir equation is determined as Eq. (6) [41]:

$$R_L = \frac{1}{1 + bC_0} \quad (6)$$

$R_L$  values between 0 and 1 indicate favorable adsorption, while  $R_L > 1$ ,  $R_L = 1$ , and  $R_L = 0$  indicate

unfavorable, linear, and irreversible adsorption processes, respectively [41]. The  $R_L$  value for nickel adsorption onto the nanostructured  $\gamma$ -alumina was found to be 0.5086, which shows favorable adsorption onto the adsorbent.

The Freundlich equation is an empirical model for multilayer adsorption onto heterogeneous surfaces of adsorbents. The linear form of the Freundlich isotherm is expressed as Eq. (7) [42]:

$$\log q_e = \log K_f + \frac{1}{n} \log C_e \quad (7)$$

where  $K_f$  and  $n$  are Freundlich constants.  $K_f$  is the adsorption coefficient and represents the adhesion ability of the adsorbate onto the adsorbent and  $n$  reflects the metal adsorption ability. Linear equilibrium, favorable, and unfavorable adsorption isotherms are reflected by  $n = 1$ ,  $n > 1$  and  $n < 1$ , respectively [43]. Since the value of  $n$  was 1.2093, it indicated favorable and almost linear adsorption.

The Tempkin isotherm equation is presented as Eq. (8) [44]:

$$q_e = B_T \ln (K_T C_e) \quad (8)$$

The isotherm can be expressed in linear form as Eq. (9):

$$q_e = B_T \ln K_T + B_T \ln C_e \quad (9)$$

$B_T$  and  $K_T$  are Tempkin empirical isotherm constants. The linear plots of the Langmuir, Freundlich and Tempkin isotherms are shown in Figs. 4–6, respectively. The parameter values of the isotherms are shown in Table 2. A comparison of the correlation coefficients ( $R^2$ ) obtained from these isotherms can be expressed as a criterion for the agreement of the experimental data with the theoretical results. The values of  $R^2$  in Table 2 indicate that Langmuir model gives a better fit to the experimental data.

As found by previous studies on the reaction mechanism, nickel predominantly chemisorbed onto the surface the nanostructured  $\gamma$ -alumina [45–47].

### 3.3. Column studies

#### 3.3.1. Breakthrough studies

A diagram of effluent concentration vs. time is known as a breakthrough curve. Initially, because of the number of available sites for the adsorbent, the ion metal effluent concentration reached its lowest value;

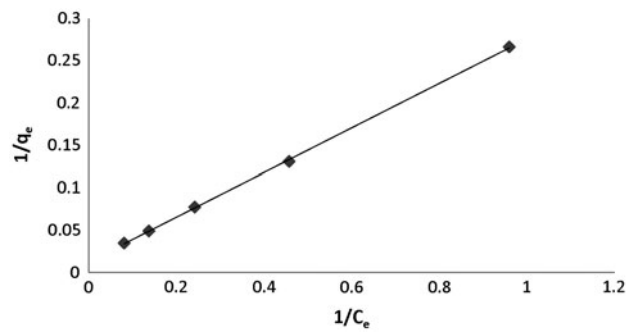


Fig. 4. Langmuir plot for adsorption of Ni (II) onto nanostructured  $\gamma$ -alumina. Conditions: adsorbent dose 5 g/L and pH 4.5.

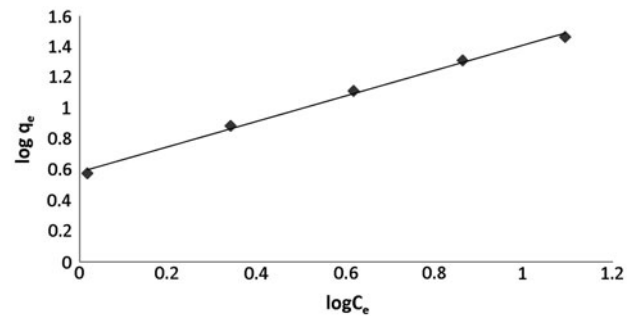


Fig. 5. Freundlich plot for adsorption of Ni (II) onto nanostructured  $\gamma$ -alumina. Conditions: adsorbent dose 5 g/L and pH 4.5.

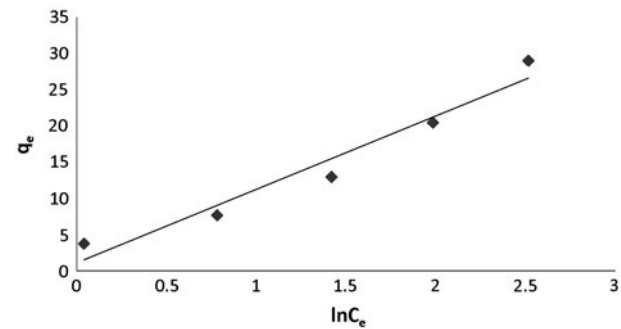


Fig. 6. Tempkin plot for adsorption of Ni (II) onto nanostructured  $\gamma$ -alumina. Conditions: adsorbent dose 5 g/L and pH 4.5.

but, over time, with the occupation of adsorbent sites by the adsorbate, the effluent concentration increased. Finally, upon adsorbate bed saturation, as time increased, the effluent concentration reached the influent concentration. In this study, the bed non-equilibrium model was used for the pore diffusion mechanism and overall mass transfer

Table 2  
Isotherm models constants

Isotherm	Parameter	Value
Langmuir	$q_{\max}$ (mg/g)	78.74
	$b$ (L/mg)	0.048
	$R^2$	0.9998
Freundlich	$1/n$	0.826
	$K_f$ (mg <sup>1-n</sup> L <sup>n</sup> g <sup>-1</sup> )	3.84
	$R^2$	0.9957
Tempkin	$B_T$	10.126
	$K_T$	1.114
	$R^2$	0.9518

coefficient. The experimental conditions for adsorption process dynamic modeling include assumptions such as:

- Concentration gradient being in the longitudinal direction.
- Regardless of the rate, fluid phase, and adsorbed phase concentration variations in the radial direction of the bed.
- Constant cross section along the bed.
- The axial dispersion diffusion from the low flow rate.
- Neglecting the pressure drop from the liquid phase.
- Constant temperature from the low concentration of adsorbate molecules.
- Neglecting surface diffusion and assuming pore diffusion because of the large pores in the adsorbent.
- Neglecting Knudsen diffusion and using molecular diffusion mechanism because of the small adsorbate molecule diameter compared with the adsorbent pore diameter.

For nanoparticles, the last two hypotheses can be considered as correct approximates in this experiment. The linear method was used to solve the partial differential equations (PDE). In this method, PDE is converted to an ordinary differential equation and only geometric derivatives were expanded, making it faster and more accurate than other numerical solution methods. The physical model is illustrated in Fig. 7.

A mathematical study of breakthrough analysis was carried out using a one-dimensional model for isothermal, non-equilibrium, axially dispersed single-component fixed-bed adsorption [28]. Partial mass balance for component  $i$  with the selection of a

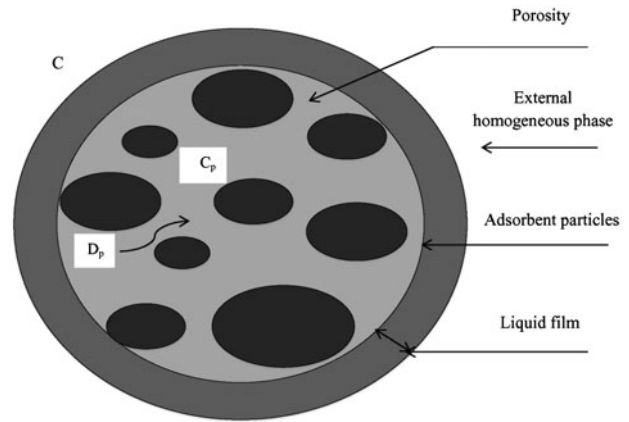


Fig. 7. Physical model of the adsorbent bed.

cylindrical element from the cylindrical bed is expressed as Eq. (10):

$$A\epsilon uC - A\epsilon D_z \frac{\partial C}{\partial z} = A\epsilon \left[ uC + \frac{\partial(uC)}{\partial z} dz \right] - A\epsilon D_z \left[ \frac{\partial C}{\partial z} + \frac{\partial^2 C}{\partial z^2} dz \right] + \text{Accumulation} \quad (10)$$

$$\text{Accumulation} = \epsilon A dz \frac{\partial C}{\partial t} + \epsilon_p \frac{\partial C_p}{\partial t} (1 - \epsilon) a dz + \rho_p \frac{\partial q}{\partial t} (1 - \epsilon) a dz \quad (11)$$

where  $C$  is bulk concentration (mol/L),  $C_p$  is pore concentration (mol/L),  $q$  is solid concentration (mg/g),  $u$  is fluid velocity (m/s),  $A$  is the cross section area of bed (m<sup>2</sup>),  $\rho_p$  is adsorbent particle density (mg/L),  $\epsilon$  is intraparticle void fraction of bed,  $\epsilon_p$  is adsorbent porosity and  $D_z$  is axial dispersion coefficient (m<sup>2</sup>/s).

In Eq. (11), the first term is the accumulation of bulk fluid inside the element, the second term is moderate accumulation of fluid in the pores of the adsorbent inside the element, and the third term is moderate accumulation of the adsorbent inside the element. By rearranging Eqs. (10) and (11), the following is obtained:

$$-D_z \frac{\partial^2 C}{\partial z^2} + \frac{\partial(uC)}{\partial z} + \frac{\partial C}{\partial t} + \frac{1 - \epsilon}{\epsilon} \left[ \epsilon_p \frac{\partial C_p}{\partial t} + \rho_p \frac{\partial q}{\partial t} \right] = 0 \quad (12)$$

$N_i$  can be expressed using different formulas and various mass transfer resistances. The fluid phase driving force concentration was used for Eq. (13) and the solid phase driving force as used for Eq. (14) [48]:

$$N_i = \frac{\partial C_p}{\partial t} \left( \varepsilon_p + \rho_p \frac{\partial q}{\partial C_p} \right) = k_i(C - C_p) \quad (13)$$

$$N_i = \rho_p \frac{\partial q}{\partial t} = k_i(q_e - q) \quad (14)$$

where  $N_i$  is mass transfer flux (mol/L.s),  $q_e$  is equilibrium solid concentration and  $k_i$  is lumped mass transfer coefficient.

Eq. (14) was used in the present study because the driving force of mass transfer is in the fluid phase. The boundary and initial conditions are:

$$B.C.1: C(z, t) = C_0 + \frac{D_z}{u} \frac{\partial C(z, t)}{\partial z}, z = 0 \quad (15a)$$

$$B.C.2: \frac{\partial C(z, t)}{\partial z} = 0, z = l \quad (15b)$$

$$C(z, 0) = 0 \quad (15c)$$

To calculate the overall mass transfer coefficient, both internal and external mass transfer resistance are added. The overall mass transfer coefficient is expressed as Eq. (16) [49]:

$$\frac{1}{K_{overall}} = \frac{R_p}{3k_f} + \frac{R_p^2}{15D_p^e \varepsilon_p} \quad (16)$$

where  $k_f$  is external mass transfer coefficient (m/s),  $D_p^e$  is effective pore diffusivity coefficient ( $m^2/s$ ) and  $R_p$  is radius of adsorbent particle (m).

The effective pore diffusivity coefficient,  $D_p^e$  is calculated as Eq. (17) [49]:

$$D_p^e = \frac{D_p}{\tau_p} \quad (17)$$

$$D_p = \frac{1}{\frac{1}{D_m} + \left(\frac{1}{D_k}\right)} \quad (18)$$

where  $D_p$  is effective pore diffusivity coefficient ( $m^2/s$ ),  $\tau_p$  is tortuosity factor,  $D_m$  is molecular diffusion coefficient ( $m^2/s$ ) and  $D_k$  is Knudsen diffusion coefficient ( $m^2/s$ ).

Because of the small diameter of the adsorbate molecule compared with the adsorbent pore diameter, the Knudsen diffusion is ignored. Thus, Eqs. (17) and (18) are simplified as:

$$D_p^e = \frac{D_m}{\tau_p} \quad (19)$$

Since the path of molecule movement into the adsorbent pores is not direct, a tortuosity factor is calculated as Eq. (20) [50]:

$$\tau_p = 1/\varepsilon_p \quad (20)$$

The Re and Sc values are in the range of experimental conditions, and there is agreement with Wakao and Funzakri; the mass transfer coefficient between the fluid and adsorbent particles is given by Eq. (21) [51]:

$$Sh = \frac{k_f d_p}{D_m} = 2 + 1.1(Sc)^{0.33}(Re)^{0.6} \quad (21)$$

This relation is valid for  $3 < Re < 10,000$  and  $0.6 < Sc < 70$ .

Since fluid velocity is low, axial dispersion is assumed for this packed bed. The axial dispersion coefficient is calculated as Eq. (22) [51]:

$$\frac{D_z}{D_m} = \gamma_1 + \gamma_2 \frac{d_p u}{D_m} = \gamma_1 + \gamma_2 \frac{(Re) \cdot (Sc)}{\varepsilon} \quad (22)$$

where  $\gamma_1 = 20/\varepsilon$  and  $\gamma_2 = 0.5$ . These values were selected because they best empirically fit the experimental results.

### 3.3.2. Effect of bed height

To study the effect of bed height on nickel removal, sorbent doses of 7.0685, 10.6028, and 14.1371 g (10, 15, and 20 cm) were placed in the column. An aqueous solution of nickel with a constant

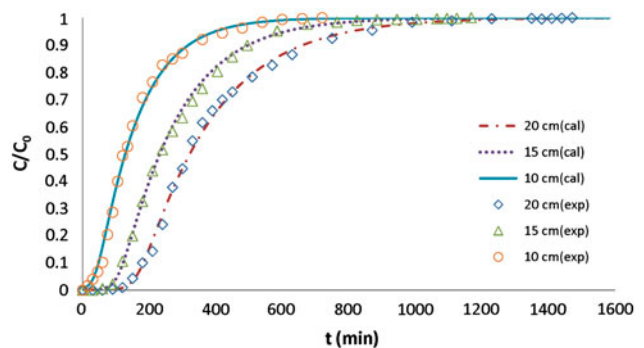


Fig. 8. Comparison of experimental breakthrough curves with theoretical in different bed heights ( $C_0 = 50 \text{ mg/L}$ ,  $Q_0 = 6 \text{ mL/min}$ ).

flow rate of 6 mL/min and constant concentration of 50 ppm passed through the column. The characteristic curves are shown in Fig. 8. Upon reaching the mass transfer zone (MTZ) at the bottom of the column, bed breakthrough occurred and nickel concentration reached that of  $C_a$  ( $C_a = 0.01 C_0$ ). The breakthrough point at bed heights of 10, 15, and 20 cm occurred at 15, 80, and 130 min, respectively. It can be concluded that the breakthrough point occurs later for greater bed heights.

The maximum adsorption capacity of nanostructured  $\gamma$ -alumina at bed heights of 10, 15, and 20 cm were 6.91, 7.95, and 8.18 mg/g, respectively. This indicates that the maximum adsorption capacity of the adsorbent increased as bed height increased. As seen in Fig. 8, the saturation times at heights of 10, 15, and 20 cm were 720, 1,168, and 1,472 min, respectively. As bed height increased from 10 to 15 to 20 cm, the saturation time increased 62.2% and 104.4%, respectively. These results revealed that increasing bed heights increases saturation time and the slope of breakthrough curve becomes gentler; thus, the MTZ develops at higher bed heights. Malkoc et al. [52] investigated the removal of Ni (II) from an aqueous solution using waste of a tea factory in a fixed-bed column. The increase in bed height from 10 to 30 cm increased adsorption capacity of the adsorbent from 10.57 to 13.6 mg/g.

### 3.3.3. Effect of flow rate

The breakthrough curve for ion metal adsorption at different flow rates, a constant influent concentration (50 ppm) and constant bed height (15 cm) is shown in Fig. 9. At flow rates of 3, 6, and 9 mL/min, the breakthrough times were 360, 80, and 30 min, respectively, and bed saturation times were 1,941, 1,168, and 742 min, respectively. As flow rate increased from 3 to 6 to 9 mL/min, saturation time decreased 39.8 and 61.7%, respectively. More contact time between the metal ions and adsorbent increased breakthrough and saturation times at lower flow rates.

At flow rates of 3, 6, and 9 mL/min, the maximum adsorption capacity of the nanostructured  $\gamma$ -alumina were 8.95, 7.95, and 7.01 mg/g, respectively; thus, metal ion adsorption per unit of mass of adsorbent increased, because there were more available active sites of adsorbent at lower flow rates.

### 3.3.4. Effect of initial nickel concentration

To study the effect of initial nickel concentration on removal efficiency of Ni(II) at different initial concentrations, bed height and flow rate were kept

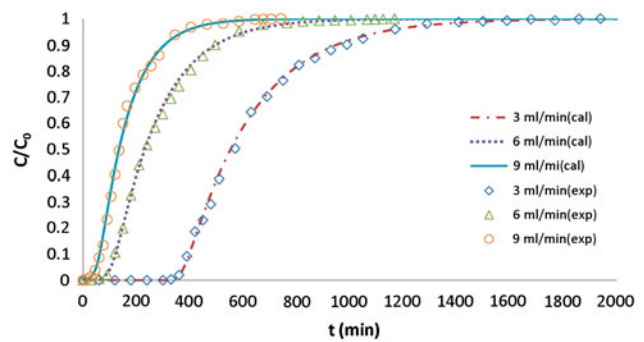


Fig. 9. Comparison of experimental breakthrough curves with theoretical in different flow rates ( $C_0 = 50$  mg/L,  $L_0 = 15$  cm).

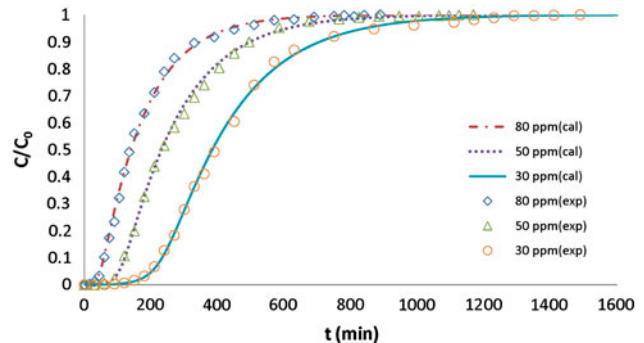


Fig. 10. Comparison of experimental breakthrough curves with theoretical in different initial concentrations ( $Q_0 = 6$  mL/min,  $L_0 = 15$  cm).

constant at 15 cm and 6 mL/min, respectively (Fig. 10). At initial nickel concentrations of 30, 50, and 80 ppm, the maximum adsorption capacity of the adsorbent was 7.48, 7.95, and 8.11 mg/g, respectively. At initial Ni(II) concentrations of 30, 50, and 80 ppm, breakthrough times were 150, 80, and 30 min and bed saturation times were 1,489, 1,168, and 888 min, respectively. Increasing initial concentration from 30 to 50 to 80 ppm, decreased saturation time 21.5 and 40.36%, respectively. The results indicate that, as influent concentration increased, the bed saturated earlier and the slope of the breakthrough curve increased.

Model parameters under various operating conditions for the fixed-bed column are listed in Table 3. The results indicate that increasing the flow rate and, consequently, increasing  $R_e$ , increased  $D_{z1}$  as shown in Eq. (22). The nickel concentration gradient decreased as initial nickel concentration increased, and thus, it can be concluded that  $D_z$  decreased. Overall, mass transfer resistance decreased as flow rate increased, thus,  $K_{overall}$  increased.

Table 3  
Lumped model parameters in the fixed bed column

$Q$ (mL/min)	$L$ (cm)	$C_0$ (mg/L)	$K_{\text{overall}}$ (1/s)	$D_z$ (m <sup>2</sup> /s)	$q_{\text{e,exp}}$ (mg/g)	$q_{\text{e,cal}}$ (mg/g)
3	15	50	$6.98 \times 10^{-5}$	$1.4732 \times 10^{-6}$	8.95	8.85
9	15	50	$1.64 \times 10^{-4}$	$1.4063 \times 10^{-4}$	7.01	6.94
6	15	50	$1.05 \times 10^{-4}$	$4.3452 \times 10^{-5}$	7.95	7.86
6	10	50	$1.47 \times 10^{-4}$	$6.9512 \times 10^{-5}$	6.91	6.81
6	20	50	$8.21 \times 10^{-5}$	$4.4671 \times 10^{-5}$	8.18	8.10
6	15	30	$9.07 \times 10^{-5}$	$5.9621 \times 10^{-5}$	7.48	7.39
6	15	80	$1.32 \times 10^{-4}$	$4.0692 \times 10^{-5}$	8.11	8.03

$K_{\text{overall}}$  increased as the metal ion concentration increased and, consequently, the concentration gradient decreased. According to Fick's law with constant mass transfer flux,  $K_{\text{overall}}$  increased.

#### 4. Conclusion

The results of this study indicate that the nanostructured  $\gamma\text{-Al}_2\text{O}_3$  has good potential for adsorbing heavy metal ion Ni (II) from aqueous solutions. The removal process is strongly dependent on contact time, solution pH, and initial solution concentration.

The effects of these parameters on nickel removal percentage were also studied. pH is an important factor affecting the adsorption efficiency. In present study, the removal efficiency of Ni (II) increased as pH increased from 2.5 to 4.5 and decreased at higher pH values. The optimum pH was determined to be 4.5. The results showed that nickel adsorption increased as contact time increased and the maximum percentage of removal was observed at 150 min.

Of the Langmuir, Freundlich and Tempkin isotherms, the Langmuir model with  $R^2 = 0.9998$  gives a better fit to the experimental data. The maximum capacity of the adsorbent in the Langmuir equation was determined to be 78.74 mg/g. The dimensionless constant of separation factor  $R_L$  was 0.5086, which shows favorable adsorption onto the adsorbent. With this value, the nanostructured  $\gamma$ -alumina was determined to be an appropriate adsorbent for the removal of nickel.

Initial nickel concentration, bed height, and flow rate were effective for the adsorption capacity of the adsorbent and shape of the breakthrough curves. The adsorption capacity of the adsorbent increased at lower flow rates, higher bed heights, and influent concentration.

From the change in the slope of the adsorption capacity under various operating conditions, it can be concluded that the effect of concentration is greater than that of bed height and the effect of bed height is

greater than that of flow rate on the removal of  $\text{Ni}^{2+}$  from an aqueous solution. Breakthrough curves with gentler slopes and increased time for saturation occurred at higher flow rates, lower bed heights, and higher influent concentration.

In the lumped method, assigning partial mass balance along the bed can describe the behavior of the breakthrough curve for the adsorption of Ni (II) ions onto nanostructured  $\gamma$ -alumina in a fixed bed column. The model included pore diffusion, surface diffusion, and axial dispersion diffusion resistances. Since surface diffusion resistance was negligible, it was ignored. Model parameters, including the overall mass transfer coefficient ( $K_{\text{overall}}$ ) and axial dispersion coefficient ( $D_z$ ), were obtained by fitting the experimental data to the theoretical model.

#### Acknowledgments

The authors wish to thank from Mr Mohammad Kavand and Mr Bagher Biralvand for their helpful supports.

#### Nomenclatures

$C_0$	—	initial concentration (mg/L)
$C_e$	—	equilibrium concentration (mg/L)
$C_t$	—	concentration in specified time (mg/L)
$C$	—	bulk concentration (mol/L)
$C_p$	—	pore concentration (mol/L)
$q_{\text{max}}$	—	maximum adsorption capacity of the adsorbent
$q_e$	—	equilibrium adsorption capacity of adsorbent (mg/g)
$q$	—	solid concentration (mg/g)
$Q$	—	flow rate (mL/min)
$L$	—	bed height (m)
$W$	—	mass of the adsorbent (g)
$V$	—	volume of metal ions solution (L)
$A$	—	cross section area of bed (m <sup>2</sup> )

$u$	— fluid velocity (m/s)
$R$	— removal percentage of metal ion from aqueous
$b$	— langmuir equilibrium constant (L/mg)
$R_L$	— dimensionless constant of separation factor
$K_f$	— freundlich constant
$n$	— freundlich constant
$B_T$	— tempkin constant
$K_T$	— tempkin constant
$\rho_p$	— adsorbent particle density (mg/L)
$\varepsilon$	— intraparticle void fraction of bed
$\varepsilon_p$	— adsorbent porosity
$N_i$	— mass transfer flux (mol/L.s)
$k_i$	— lumped mass transfer coefficient
$k_f$	— external mass transfer coefficient (m/s)
$K_{overall}$	— overall mass transfer coefficient (1/s)
$d_p$	— diameter of adsorbent particle (m)
$R_p$	— radius of adsorbent particle (m)
$D_z$	— axial dispersion coefficient (m <sup>2</sup> /s)
$D_p^e$	— effective pore diffusivity coefficient (m <sup>2</sup> /s)
$D_p$	— effective pore diffusivity coefficient (m <sup>2</sup> /s)
$D_m$	— molecular diffusion coefficient (m <sup>2</sup> /s)
$D_k$	— knudsen diffusion coefficient (m <sup>2</sup> /s)
$\tau_p$	— tortuosity factor

## References

- [1] K. Kadirvelu, K. Thamaraiselvi, C. Namasivayam, Adsorption of nickel (II) from aqueous solution onto activated carbon prepared from coirpith, *Sep. Purif. Technol.* 24 (2001) 497–505.
- [2] A.F. Ngomsik, A. Bee, J.M. Siaugue, D. Talbot, V. Cabuil, G. Cote, Co (II) removal by magnetic alginate beads containing Cyanex 272, *J. Hazard. Mater.* 166 (2009) 1043–1049.
- [3] J. Wang, C. Chen, Biosorbents for heavy metals removal and their future, *Biotechnol. Adv.* 27 (2009) 195–226.
- [4] P. Yin, Q. Xu, R. Qu, G. Zhao, Y. Sun, Adsorption of transition metal ions from aqueous solutions onto a novel silica gel matrix inorganic–organic composite material, *J. Hazard. Mater.* 173 (2010) 710–716.
- [5] K. Kadirvelu, P. Senthilkumar, K. Thamaraiselvi, V. Subburam, Activated carbon prepared from biomass as adsorbent: Elimination of Ni(II) from aqueous solution, *Biores. Technol.* 81 (2002) 87–90.
- [6] USEPA, National Primary Drinking Water Regulations, Ground Water and Drinking Water, Consumer Factsheet on: NICKEL, 1995. <http://www.epa.gov/ogwdw/dwh/t-ioc/nickel.html>
- [7] L. Marder, G.O. Sulzbach, A.M. Bernardes, J.Z. Ferreira, Removal of cadmium and cyanide from aqueous solutions through electrodialysis, *J. Braz. Chem. Soc.* 14 (2003) 610–615.
- [8] H.B. Bradl, Adsorption of heavy metal ions on soils and soils constituents, *J. Colloid Interface Sci.* 277 (2004) 1–18.
- [9] A.M.Y. Chong, Y.S. Wong, N.F.Y. Tam, Performance of different microalgal species in removing nickel and zinc from industrial wastewater, *Chemosphere* 41 (2000) 251–257.
- [10] S. Ricordel, S. Taha, I. Cisse, G. Dorange, Heavy metal removal by adsorption onto peanut husks carbon, *Sep. Purif. Technol.* 24 (2001) 389–401.
- [11] D.W. O’Connell, C. Birkinshaw, T.F. O’Dwyer, Heavy metal adsorbents prepared from the modification of cellulose, *J. Biores. Technol.* 99 (2008) 6709–6724.
- [12] M.A.O. Badmus, T.O.K. Audu, B.U. Anyata, Removal of heavy metal from industrial wastewater using hydrogen peroxide, *Afr. J. Biotechnol.* 6 (2007) 238–242.
- [13] F. Fu, Q. Wang, Removal of heavy metal ions from wastewaters: A review, *J. Environ. Manage.* 92 (2010) 407–418.
- [14] D. Mohan, K.P. Singh, Single- and multi-component adsorption of cadmium and zinc using activated carbon derived from bagasse—An agricultural waste, *J. Water Res.* 36 (2002) 2304–2318.
- [15] T. Motsi, N.A. Rowson, M.J.H. Simmons, Adsorption of heavy metals from acid mine drainage by natural zeolite, *Int. J. Miner. Process.* 92 (2009) 42–48.
- [16] C.A. R’ios, C.D. Williams, C.L. Roberts, Removal of heavy metals from acid mine drainage (AMD) using coal fly ash, natural clinker and synthetic zeolites, *J. Hazard. Mater.* 156 (2008) 23–35.
- [17] H. Genc-Fuhrman, P.S. Mikkelsen, A. Ledin, Simultaneous removal of As, Cd, Cr, Cu, Ni, and Zn from stormwater: Experimental comparison of 11 different sorbents, *Water Res.* 41 (2007) 591–602.
- [18] B. Geng, Z. Jin, T. Li, X. Qi, Kinetics of hexavalent chromium removal from water by chitosan-Fe nanoparticles, *J. Chemosphere* 75 (2009) 825–830.
- [19] M. Ahmedna, W.E. Marshall, A.A. Husseiny, R.M. Rao, I. Goktepe, The use of nutshell carbons in drinking water filters for removal of trace metals, *Water Res.* 38 (2004) 1062–1068.
- [20] L. Zhang, T. Huang, M. Zhang, X. Guo, Z. Yuan, Studies on the capability and behavior of adsorption of thallium on nano-Al<sub>2</sub>O<sub>3</sub>, *J. Hazard. Mater.* 157 (2008) 352–357.
- [21] J. Lu, F. Xu, W. Cai, Adsorption of MTBE on nano zeolite composites of selective supports, *Microporous Mesoporous Mater.* 108 (2008) 50–55.
- [22] E. Pehlivan, G. Arslan, Removal of metal ions using lignite in aqueous solution low cost biosorbents, *J. Fuel Process Technol.* 88 (2007) 99–106.
- [23] V.S. Munagapati, V. Yarramuthi, S.K. Nadavala, S.R. Alla, K. Abburi, Biosorption of Cu (II), Cd(II) and Pb(II) by *Acacia leucocephala* bark powder: Kinetics, equilibrium and thermodynamics, *Chem. Eng. J.* 157 (2010) 357–365.
- [24] W. Qiu, Y. Zheng, Removal of lead, copper, nickel, cobalt, and zinc from water by a cancrinite-type zeolite synthesized from fly ash, *Chem. Eng. J.* 145 (2009) 483–488.
- [25] A.-F. Ngomsik, A. Bee, M. Draye, G. Cote, V. Cabuil, Magnetic nano- and microparticles for metal removal and environmental applications, *J. Chim.* 8 (2005) 963–970.
- [26] J. Li, Y. Shi, Y. Cai, S. Moua, G. Jiang, Adsorption of di-ethyl-phthalate from aqueous solutions with surfactant-coated nano/microsized alumina, *Chem. Eng. J.* 140 (2008) 214–220.

- [27] M. Hiraide, J. Iwasawa, S. Hiramatsu, H. Kawaguchi, Use of surfactant aggregates form on alumina for the preparation of chelating sorbents, *Anal. Sci.* 11 (1995) 611–615.
- [28] S. Ghorai, K.K. Pant, Investigations on the column performance of fluoride adsorption by activated alumina in a fixed-bed, *Chem. Eng. J.* 98 (2004) 165–173.
- [29] A. Adak, A. Pal, Removal of phenol from aquatic environment by SDS-modified alumina: Batch and fixed bed studies, *Sep. Purif. Technol.* 50 (2006) 256–262.
- [30] K.-M. Hong, M.-S. Kim, J.G. Chung, Adsorption characteristics of Ni (II) on c-type alumina particles and its determination of overall adsorption rate by a differential bed reactor, *Chemosphere* 54 (2004) 927–934.
- [31] A. Afkhami, M.S. Tehrani, H. Bagheri, Simultaneous removal of heavy-metal ions in wastewater samples using nano-alumina modified with 2,4-dinitrophenylhydrazine, *J. Hazard. Mater.* 181 (2010) 836–844.
- [32] A. Rahmani, H.Z. Mousavi, M. Fazli, Effect of nano-structure alumina on adsorption of heavy metals, *Desalination* 253 (2010) 94–100.
- [33] E.I. Unuabonah, M.I. El-Khaiary, B.I. Olu-Owolabi, Predicting the dynamics and performance of a polymer-clay based composite in a fixed bed system for the removal of lead (II) ion, *Chem. Eng. Res. Design* 90 (2012) 1105–1115.
- [34] R.L. Ramos, L.A.B. Jacome, J.M. Barron, L.F. Rubio, R.M.G. Coronado, Adsorption of zinc(II) from aqueous solution onto activated carbon, *J. Hazard. Mater., B* 90 (2002) 27–38.
- [35] F. Pagnanelli, A. Esposito, L. Toro, F. Vegliò, Metal speciation and pH effect on Pb, Cu, Zn and Cd biosorption onto *Sphaerotilus natans*: Langmuir-type empirical model, *Water Res.* 37 (2003) 627–633.
- [36] Z. Reddad, C. Gerente, Y. Andres, P. Le Cloirec, Adsorption of several metal ions onto a low-cost biosorbent: Kinetic and equilibrium studies, *Environ. Sci. Technol.* 36 (2002) 2067–2073.
- [37] H.Z. Freundlich, Over the adsorption in solution, *J. Phys. Chem.* 57 (1906) 385–470.
- [38] I. Langmuir, The adsorption of gases on plane surfaces of glass, mica and platinum, *J. Am. Chem. Soc.* 40 (1918) 1361–1403.
- [39] W. Jianlong, Z. Xinmin, D. Decai, Z. Ding, Bioadsorption of lead(II) from aqueous solution by fungal biomass of *Aspergillus niger*, *J. Biotechnol.* 87 (2001) 273–277.
- [40] I. Langmuir, The constitution and fundamental properties of solids and liquids, *J. Am. Chem. Soc.* 38 (1916) 2221–2295.
- [41] G. McKay, H.S. Blair, J.R. Gardener, Adsorption of dyes on chitin. I. Equilibrium studies, *J. Appl. Polym. Sci.* 27 (1982) 3043–3057.
- [42] G. García, Á. Faz, M. Cunha, Performance of *Piptatherum miliaceum* (Smilo grass) in edaphic Pb and Zn phytoremediation over a short growth period, *Int. Biodeterior. Biodegrad.* 54 (2004) 245–250.
- [43] M.M. Rao, D.K. Ramana, K. Seshiah, M.C. Wang, S.W.C. Chien, Removal of some metal ions by activated carbon prepared from *Phaseolus aureus* hulls, *J. Hazard. Mater.* 166 (2009) 1006–1013.
- [44] A. Şeker, T. Shahwan, A.E. Eroğlu, S. Yılmaz, Z. Demirel, M. Conk Dalay, Equilibrium, thermodynamic and kinetic studies for the biosorption of aqueous lead(II), cadmium(II) and nickel(II) ions on *Spirulina platensis*, *J. Hazard. Mater.* 154 (2008) 973–980.
- [45] G.D. Gatta, B. Fubini, G. Ghiotti, C. Morterra, The chemisorption of carbon monoxide on various transition aluminas, *J. Catal.* 43 (1976) 90–98.
- [46] S. Cai, K. Sohlberg, Adsorption of alcohols on  $\gamma$ -alumina (1 1 0 C), *J. Mol. Catal. A: Chem.* 193 (2003) 157–164.
- [47] A. Iannibello, S. Marengo, A Study of the chemisorption of chromium (VI), molybdenum (VI) and tungsten (VI) onto  $\gamma$ -alumina, *Stud. Surf. Sci. Catal.* 3 (1979) 65–76.
- [48] M. Siahpoosh, S. Fatemi, A. Vatani, Mathematical modeling of single and multi-component adsorption fixed beds to rigorously predict the mass transfer zone and breakthrough curves, *Iran. J. Chem. Chem. Eng.* 28 (2009) 25–44.
- [49] R.T. Yang, *Gas separation by Adsorption Processes*, Butterworths, Boston, 1987, pp. 9–39.
- [50] N. Wakao, J.M. Smith, Diffusion in catalyst pellets, *Chem. Eng. Sci.* 17 (1962) 825.
- [51] N. Wakao, T. Funazkri, Effect of fluid dispersion coefficients on particle-fluid mass transfer coefficients in packed bed, *Chem. Eng. Sci.* 33 (1978) 1375–1384.
- [52] E. Malkoc, Y. Nuhoglu, Removal of Ni (II) ions from aqueous solutions using waste of tea factory: Adsorption on a fixed-bed column, *J. Hazard. Mater.* 135 (2006) 328–336.